

Regeneration and experimental orthotopic transplantation of a bioengineered kidney

Jeremy J Song^{1,2}, Jacques P Guyette^{1,2}, Sarah E Gilpin^{1,2}, Gabriel Gonzalez^{1,2}, Joseph P Vacanti¹⁻³ & Harald C Ott^{1,2,4}

Approximately 100,000 individuals in the United States currently await kidney transplantation, and 400,000 individuals live with end-stage kidney disease requiring hemodialysis. The creation of a transplantable graft to permanently replace kidney function would address donor organ shortage and the morbidity associated with immunosuppression. Such a bioengineered graft must have the kidney's architecture and function and permit perfusion, filtration, secretion, absorption and drainage of urine. We decellularized rat, porcine and human kidneys by detergent perfusion, yielding acellular scaffolds with vascular, cortical and medullary architecture, a collecting system and ureters. To regenerate functional tissue, we seeded rat kidney scaffolds with epithelial and endothelial cells and perfused these cell-seeded constructs in a whole-organ bioreactor. The resulting grafts produced rudimentary urine *in vitro* when perfused through their intrinsic vascular bed. When transplanted in an orthotopic position in rat, the grafts were perfused by the recipient's circulation and produced urine through the ureteral conduit *in vivo*.

Nearly 1 million patients in the United States live with end-stage renal disease (ESRD), with over 100,000 new diagnoses every year¹. Although hemodialysis has increased the survival of patients with ESRD, transplantation remains the only available curative treatment. About 18,000 kidney transplants are performed per year in the United States¹, yet approximately 100,000 Americans currently await a donor kidney². Stagnant donor organ numbers have increased waiting times to over 3 years and waitlist mortality to 5–10%. Despite advances in renal transplant immunology³, 20% of recipients will experience an episode of acute rejection within 5 years of transplantation, and approximately 40% of recipients will die or lose graft function within 10 years after transplantation. Creation of a bioengineered kidney could theoretically bypass these problems by providing an autologous graft on demand.

Hemofiltration and hemodialysis use an acellular semipermeable membrane to substitute the native kidney's functions. Several attempts have been made to bioengineer viable tubular structures to further supplement hemofiltration with cell-dependent functions^{4,5}. When hemofiltration devices have been combined with bioengineered renal

tubules, the resulting bioartificial kidney replaced renal function in uremic dogs⁶ and temporarily improved renal function in patients with acute renal failure^{7,8}. In an alternative approach, kidney primordia have been shown to develop into functional organs *in vivo* and prolong life when transplanted into anephric rats⁹. Devices to make renal-assist devices more portable¹⁰ or even implantable¹¹ have reached the stage of preclinical evaluation and hold tremendous promise for improving the quality of life of patients in end-stage renal failure. Autologous urinary tract tissue generated from biocompatible matrix and patient-derived cells has been used clinically for bladder augmentation¹². A key step toward a fully implantable, permanent graft is the development of a biocompatible scaffold that facilitates cell engraftment and function and allows full recipient integration through blood perfusion.

On the basis of our previous experience with whole-organ heart¹³ and lung¹⁴ extracellular matrix (ECM) scaffolds, we hypothesized that the native kidney ECM could provide such a scaffold for subsequent cell seeding. In previous studies, detergents were used to remove cells from native kidney ECM while preserving the biomechanical properties and matrix protein characteristics in tissue slices¹⁵ and whole organs¹⁶⁻¹⁹. We therefore decellularized kidneys using detergent perfusion to create whole-organ scaffolds with intact and perfusable vascular, glomerular and tubular compartments. We repopulated the decellularized kidney scaffolds with endothelial and epithelial cells. *In vitro* biomimetic culture using arterial perfusion led to the formation of functional renal grafts. To test *in vivo* host integration and function, we transplanted bioengineered kidneys in an orthotopic position and documented urine production.

RESULTS

Perfusion decellularization of cadaveric kidneys

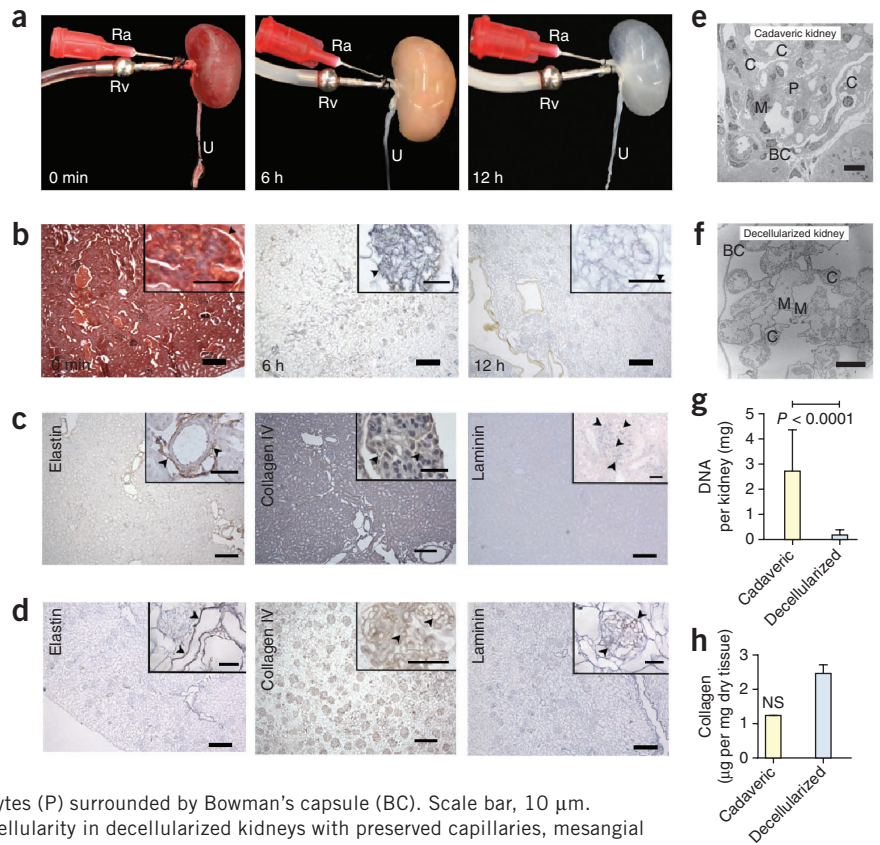
We decellularized cadaveric rat kidneys using renal artery perfusion with 1% sodium dodecyl sulfate (SDS) at a constant pressure of 40 mm Hg (**Fig. 1a**). Histology of the acellular kidneys showed preservation of tissue architecture and the complete removal of nuclei and cellular components (**Fig. 1b**). Perfusion decellularization preserved the structure and composition of the renal ECM, which is integral in filtration (glomerular basement membrane), secretion and reabsorption (tubular basement membrane). As has been seen with other tissues^{13,14}, the arterial elastic fiber network remained preserved in

¹Center for Regenerative Medicine, Massachusetts General Hospital, Boston, Massachusetts, USA. ²Harvard Medical School, Boston, Massachusetts, USA.

³Department of Surgery, Division of Pediatric Surgery, Massachusetts General Hospital, Boston, Massachusetts, USA. ⁴Department of Surgery, Division of Thoracic Surgery, Massachusetts General Hospital, Boston, Massachusetts, USA. Correspondence should be addressed to H.C.O. (hott@partners.org).

Received 4 September 2012; accepted 11 February 2013; published online 14 April 2013; doi:10.1038/nm.3154

Figure 1 Perfusion decellularization of whole rat kidneys. **(a)** Time-lapse photographs of a cadaveric rat kidney undergoing antegrade renal arterial perfusion decellularization. Shown are a freshly isolated kidney (left) and the same kidney after 6 h (middle) and 12 h (right) of SDS perfusion. Ra, renal artery; Rv, renal vein; U, ureter. **(b)** Representative corresponding Movat's pentachrome-stained sections of rat kidney during perfusion decellularization (black arrowheads indicate the Bowman's capsule). Scale bars, 250 μ m (main images); 50 μ m (insets). **(c)** Representative immunohistochemical stains of cadaveric rat kidney sections showing the distribution of elastin (black arrowheads indicate elastic fibers in the tunica media of cortical vessels), collagen IV and laminin (black arrowheads indicate the glomerular basement membranes). Scale bars, 250 μ m (main images); 50 μ m (insets). **(d)** Corresponding sections of decellularized rat kidney tissue after immunohistochemical staining for elastin, collagen IV and laminin confirming the preservation of extracellular matrix proteins in the absence of cells. Black arrowheads indicate the preserved vascular and glomerular basement membranes. Scale bars, 250 μ m (main images); 50 μ m (insets). **(e)** Transmission electron micrograph (TEM) of a cadaveric rat glomerulus showing capillaries (C), the mesangial matrix (M) and podocytes (P) surrounded by Bowman's capsule (BC). Scale bar, 10 μ m. **(f)** TEM of decellularized rat glomerulus showing acellularity in decellularized kidneys with preserved capillaries, mesangial matrix and Bowman's space encapsulated by Bowman's capsule. Scale bar, 10 μ m. **(g,h)** Biochemical quantification of DNA and total collagen in cadaveric and decellularized rat kidney tissue showing a reduction of DNA content and a preservation of collagen after perfusion decellularization. Data are shown as the mean \pm s.d. NS, not significant. Statistical significance was determined by Student's *t* test.



acellular cortical and medullary parenchyma. Immunohistochemical staining confirmed the presence of key ECM components such as laminin and collagen IV in a physiologic distribution, for example, in the acellular glomerular basement membrane (Fig. 1c,d). The microarchitecture of the lobulated glomerular basement membrane with the capillary and mesangial matrix extending from the centrilobular stalk remained intact. Acellular glomeruli were further encompassed by a multilayered corrugated and continuous Bowman's capsule basement membrane (Fig. 1e,f). Tubular basement membranes remained preserved, with dentate evaginations extending into the proximal tubular lumen. SDS, deionized water and Triton X-100 reduced the total DNA content per kidney to less than 10% (Fig. 1g). After washing with PBS, SDS was undetectable in the acellular kidney scaffolds. Concentrations of total collagen and glycosaminoglycans in the ECM were preserved at levels not significantly different from those in cadaveric kidney tissue (Fig. 1h). To confirm the scalability of the perfusion decellularization protocol to kidneys of large animals and humans, we successfully decellularized porcine and human kidneys using a similar perfusion protocol (Fig. 2a–d). We confirmed preservation of perfusable channels along a hierarchical vascular bed by dye perfusion in a manner similar to that in our previous experiments with perfusion of decellularized hearts and lungs^{13,14} (Supplementary Fig. 1). Functional testing of acellular kidney scaffolds by perfusion of the vasculature with modified Krebs-Henseleit solution under physiologic perfusion pressure resulted in production of a filtrate that was high in protein, glucose and electrolytes, suggesting hydrostatic filtration across glomerular and tubular basement membranes with loss of macromolecular sieving and active reabsorption.

To assess the microarchitecture of the acellular kidney scaffolds, we applied an established histology-based morphometry protocol to quantify the average number of glomeruli, glomerular diameter, glomerular capillary lumen and partial Bowman's space²⁰. The total number of glomeruli remained unchanged between cadaveric and decellularized kidney cross sections through the hilum ($12,380.25 \pm 967.37$ (mean \pm s.d.) compared to $14,790.35 \pm 2,504.93$, respectively; $P = 0.931$). Glomerular diameter, Bowman's space and glomerular capillary surface area did not differ between cadaveric and decellularized kidneys (Supplementary Table 1).

Recellularization of acellular kidney scaffolds

To regenerate functional kidney tissue, we repopulated acellular rat kidneys with endothelial and epithelial cells. We instilled suspended human umbilical venous endothelial cells (HUVECs) through the renal artery and suspended rat neonatal kidney cells (NKC) through the ureter. Cell delivery and retention improved when kidney scaffolds were mounted in a seeding chamber under a vacuum to generate a pressure gradient across the scaffold (Fig. 3a). Attempts to seed NKC by applying positive pressure to the collecting system did not reach the glomerulus, whereas cell seeding using a transrenal gradient allowed for cell dispersion throughout the entire kidney parenchyma. Vacuum pressure exceeding 70 cm H₂O led to tissue damage in the calyces and parenchyma, but a vacuum pressure of 40 cm H₂O did not cause macroscopic or microscopic tissue damage or leakage of cells, which is consistent with data on isolated tubular basement membrane mechanical properties²¹. After seeding, we transferred kidney constructs to a perfusion bioreactor designed to provide whole-organ

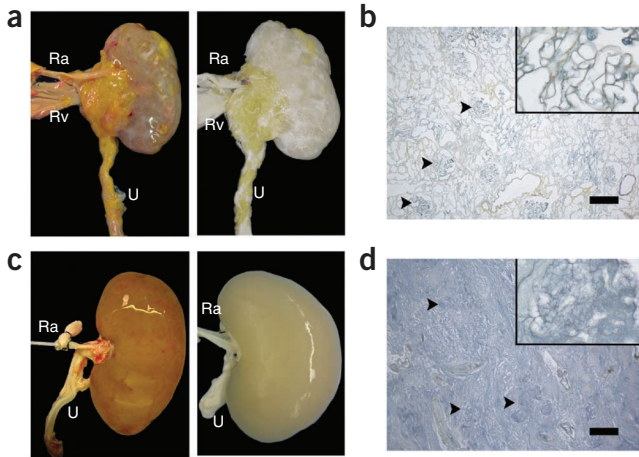


Figure 2 Perfusion decellularization of porcine and human kidneys. (a) Photograph of cadaveric (left) and decellularized (right) porcine kidneys suggesting that perfusion decellularization of rat kidneys can be upscaled to generate acellular kidney ECMs of clinically relevant size. Ra, renal artery; Rv, renal vein; U, ureter. (b) Corresponding pentachrome staining for decellularized porcine kidneys (black arrowheads indicate acellular glomeruli). Scale bar, 250 μm ; insets are $\times 40$ magnification. (c) Photograph of cadaveric (left) and decellularized (right) human kidneys. (d) Corresponding pentachrome staining for decellularized human kidneys (black arrowheads indicate acellular glomeruli). Scale bar, 250 μm ; insets are $\times 40$ magnification.

culture conditions (Fig. 3b,c). After 3–5 d of perfused organ culture, HUVECs lined the vascular channels throughout the entire scaffold cross section from segmental, interlobar and arcuate arteries to glomerular and peritubular capillaries (Fig. 3d).

Because a variety of epithelial cell phenotypes in different niches along the nephron contribute to urine production, we elected to reseed a combination of rat NKC through the ureter in addition to HUVECs through the renal artery. Freshly isolated, enzymatic digests of rat neonatal kidneys produced single-cell suspensions of NKC consisting of a heterogeneous mixture of all kidney cell types, most of which were of epithelial lineage but some of which were of endothelial and interstitial lineages. When cultured on cell-culture plastic after isolation, 8% of adherent cells expressed podocin, indicating a glomerular epithelial phenotype, 69% expressed Na/K-ATPase, indicating a proximal tubular phenotype, and 25% expressed E-cadherin, indicating a distal tubular phenotype (data not shown). After cell seeding, we mounted the kidney constructs in a perfusion bioreactor and cultured them in whole-organ biomimetic culture. An initial period of static culture enabled cell attachment, after which we initiated perfusion to provide oxygenation, nutrient supply and a filtration stimulus.

Neonatal rats are unable to excrete concentrated urine due to immaturity of the tubular apparatus²². To accelerate *in vitro* nephrogenesis and maturation of NKC in acellular kidney matrices, we supplemented the culture medium with *in vivo* maturation signals such as glucocorticoids and catecholamines. We cultured the reseeded kidneys under physiologic conditions for up to 12 d. By histologic evaluation after as early as 4 d in culture, we found repopulation of the renal scaffold with epithelial and endothelial cells and preservation of glomerular, tubular and vascular architecture. NKC and HUVECs engrafted in their appropriate epithelial and vascular compartments (Fig. 3e). The spatial relationship of the regenerated epithelium and endothelium resembled the microanatomy and polarity of the native

nephron, providing the anatomic basis for water and solute filtration, secretion and reabsorption. Immunostaining revealed densely seeded glomeruli with endothelial cells and podocytes. Across the entire kidney, podocytes seemed to preferentially engraft in glomerular regions, although we did find occasional non-site specific engraftment (Fig. 3f,g). Epithelial cells on the glomerular basement membranes stained positive for β -1 integrin, suggesting site-specific cell adhesion to ECM domains (Fig. 3h). We found that engrafted epithelial cells reestablished polarity and organized in tubular structures expressing Na/K-ATPase and aquaporin, which is similar to native proximal tubular epithelium. Epithelial cells expressing E-cadherin formed structures resembling native distal tubular epithelium and collecting ducts (Fig. 3e,h). E-cadherin-positive epithelial cells lined the renal pelvis, which is similar to native transitional epithelium. Transmission and scanning electron microscopy of regenerated kidneys showed perfused glomerular capillaries with engrafted podocytes and formation of foot processes (Fig. 3i,j). Morphometric analysis of regenerated kidneys showed recellularization of more than half of the glomerular matrices, resulting in an average number of cellular glomeruli per regenerated kidney that was approximately 70% that of cadaveric kidneys. The average glomerular diameter, Bowman's space and glomerular capillary lumen were smaller in regenerated kidneys compared to cadaveric kidneys (Supplementary Table 2).

In vitro function of acellular and regenerated kidneys

After cell seeding and whole-organ culture, we tested the *in vitro* capacity of regenerated kidneys to filter a standardized perfusate, clear metabolites, reabsorb electrolytes and glucose and generate concentrated urine (Fig. 4a). Decellularized kidneys produced nearly twice as much filtrate as cadaveric controls, and regenerated kidneys produced the least amount of urine. All three groups maintained a steady urine output over the testing period (Fig. 4b). On the basis of the results of urinalysis, we calculated creatinine clearance as an estimate for glomerular filtration rate and fractional solute excretion as a measure of tubular absorptive and secretory function (Fig. 4c). Because of increased dilute urine production, the calculated creatinine clearance was increased in decellularized kidneys when compared to cadaveric kidneys, indicating increased glomerular (and probably additional tubular and ductal) filtration across acellular basement membranes. After repopulation with endothelial and epithelial cells, creatinine clearance of regenerated constructs reached approximately 10% of that in cadaveric kidneys, which indicates a decrease of glomerular filtration across a partially reconstituted and probably immature glomerular membrane (Fig. 4c).

We found that vascular resistance increased with decellularization and decreased after re-endothelialization, but it remained higher in regenerated constructs compared to cadaveric kidneys (Fig. 4d). This finding is in line with previous observations in cardiac and pulmonary re-endothelialization^{13,14} and may be related to the relative immaturity of the vascular bed and microemboli from cell-culture medium. When we increased the *in vitro* renal arterial perfusion pressure to 120 mm Hg, urine production and creatinine clearance in regenerated kidneys reached up to 23% of that in cadaveric kidneys (Fig. 4b,c). Albumin retention was decreased from 89.9% in cadaveric kidneys to 23.3% in decellularized kidneys, which is an amount consistent with the estimated contribution of the denuded glomerular basement membrane to macromolecular sieving. With recellularization, albumin retention was partially restored to 46.9%, leading to improved albuminuria in regenerated kidneys. Glucose reabsorption decreased from 91.7% in cadaveric kidneys to 2.8% after

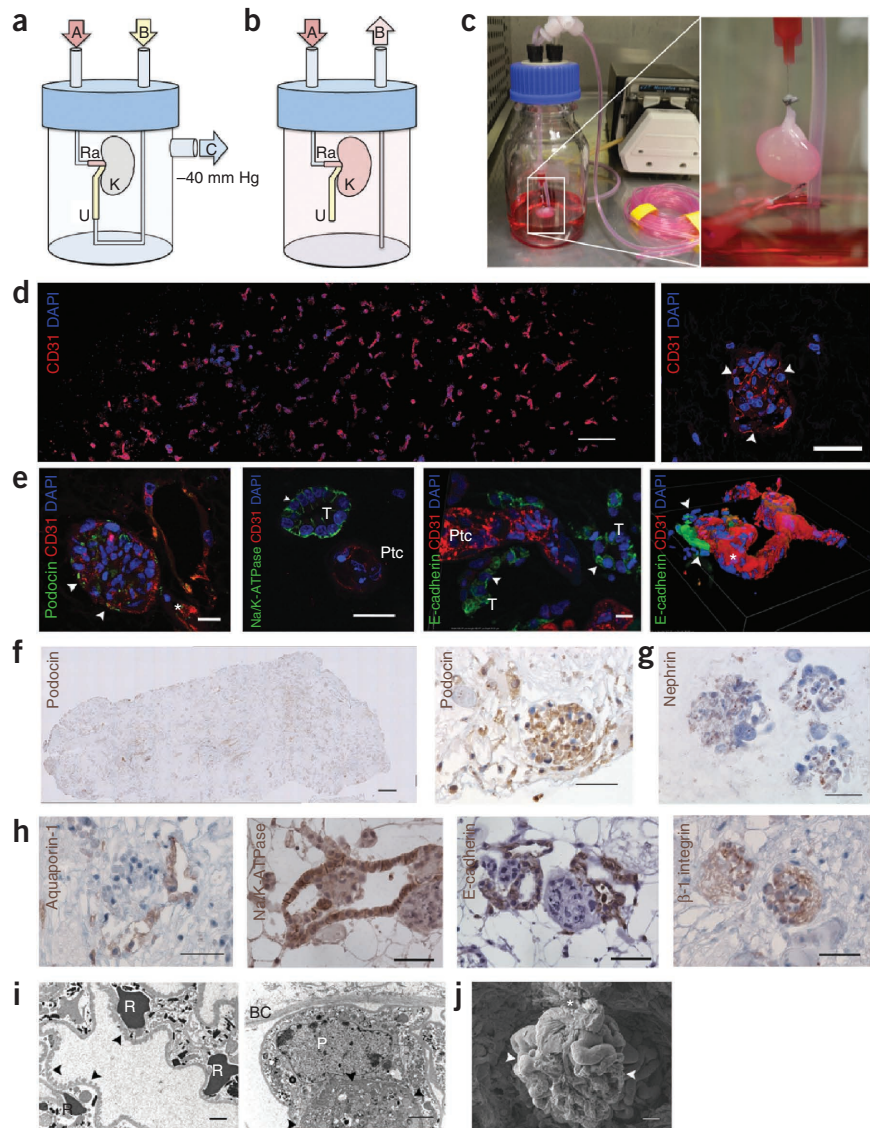


TECHNICAL REPORTS

Figure 3 Cell seeding and whole-organ culture of decellularized rat kidneys. **(a)** Schematic of a cell-seeding apparatus enabling endothelial cell seeding through port A attached to the renal artery (Ra) and epithelial cell seeding through port B attached to the ureter (U) while negative pressure in the organ chamber is applied to port C, thereby generating a transrenal pressure gradient. **(b)** Schematic of a whole-organ culture in a bioreactor enabling tissue perfusion through port A attached to the renal artery and drainage to a reservoir through port B. K, kidney. **(c)** Cell-seeded decellularized rat kidney in whole-organ culture. **(d)** Fluorescence micrographs of a re-endothelialized kidney constructs.

CD31-positive (red) and DAPI-positive HUVECs line the vascular tree across the entire graft cross section (image reconstruction, left) and form a monolayer to glomerular capillaries (right; white arrowheads indicate endothelial cells). Scale bar, 500 μ m (left); 50 μ m (right).

(e) Fluorescence micrographs of re-endothelialized and re-epithelialized kidney constructs showing engraftment of podocin-expressing cells (green) and endothelial cells (CD31 positive; red) in a glomerulus (left; white arrowheads indicate Bowman's capsule and the asterisk indicates the vascular pole); engraftment of Na/K-ATPase-expressing cells (green) in a basolateral distribution in tubuli resembling proximal tubular structures with the appropriate nuclear polarity (left middle); engraftment of E-cadherin-expressing cells in tubuli resembling distal tubular structures (right middle); and a three-dimensional reconstruction of a re-endothelialized vessel leading into a glomerulus (white arrowheads indicate Bowman's capsule, and the asterisk indicates the vascular pole). T, tubule; Ptc, peritubular capillary. Scale bar, 25 μ m (left); 10 μ m (middle and right). **(f)** Image reconstruction of an entire graft cross section confirming engraftment of podocin-expressing epithelial cells (left) and representative immunohistochemical staining of a reseeded glomerulus showing podocin expression (right). Scale bar, 500 μ m (left); 50 μ m (right). **(g)** Nephrin expression in regenerated glomeruli. Scale bar, 50 μ m. **(h)** Aquaporin-1 expression in regenerated proximal tubular structures (left); Na/K-ATPase expression in regenerated proximal tubular epithelium (middle left); E-cadherin expression in regenerated distal tubular epithelium (middle right); and β -1 integrin expression in a regenerated glomerulus (right). Scale bars, 50 μ m. **(i)** Representative TEM of a regenerated glomerulus showing a capillary with red blood cells (R) and foot processes along the glomerular basement membrane (black arrowheads; left) and TEM of a podocyte (P) adherent to the glomerular basement membrane (black arrowheads; right). BC, Bowman's capsule. Scale bars, 2 μ m. **(j)** Scanning electron micrograph of a glomerulus (white arrowheads) in a regenerated kidney graft cross section. The asterisk indicates a vascular pedicle. Scale bar, 10 μ m.



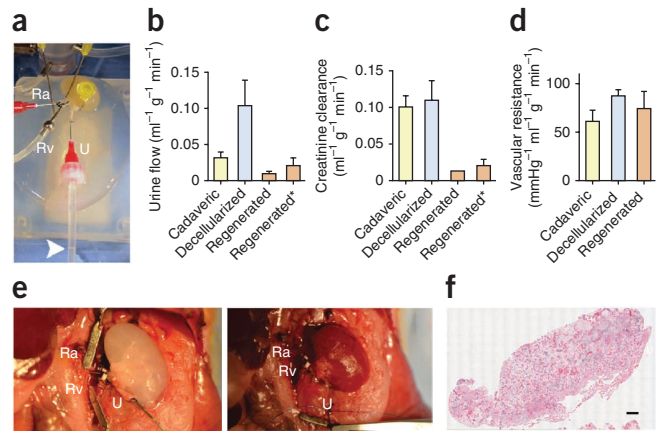
decellularization, consistent with free filtration and the loss of tubular epithelium. Regenerated kidneys showed partially restored glucose reabsorption of 47.38%, suggesting engraftment of proximal tubular epithelial cells with functional membrane transporters, resulting in decreased glucosuria. Higher perfusion pressure did not lead to increased albumin or glucose loss in regenerated kidneys. Selective electrolyte reabsorption was lost in decellularized kidneys. Slightly more creatinine than electrolytes were filtered, leading to an effective fractional electrolyte retention ranging from 5% to 10%. This difference may be attributed to the electrical charge of the retained ions and the basement membrane²³, whereas the range among ions may be related to subtle differences in diffusion dynamics across acellular vascular, glomerular and tubular basement membranes. In regenerated

kidneys, electrolyte reabsorption was restored to approximately 50% of physiologic levels, which further indicates engraftment and function of proximal and distal tubular epithelial cells. Fractional urea excretion was increased in decellularized kidneys and returned to a more physiologic range in regenerated kidneys, which suggests partial reconstitution of functional collecting duct epithelium with urea transporters. For further details about the urinalysis and fractional excretion, see **Supplementary Table 3**.

Orthotopic transplantation of regenerated kidneys

Because we observed urine production *in vitro*, we hypothesized that regenerated kidneys could function *in vivo* after orthotopic transplantation. We performed experimental left nephrectomies

Figure 4 *In vitro* function of bioengineered kidney grafts and orthotopic transplantation. **(a)** Photograph of a bioengineered rat kidney construct undergoing *in vitro* testing. The kidney is perfused through the cannulated renal artery (Ra) and renal vein (Rv), while urine is drained through the ureter (U). The white arrowhead indicates the urine-air interface in the drainage tubing. **(b)** Bar graph summarizing average urine flow rate (ml min^{-1}) for decellularized, cadaveric and regenerated kidneys perfused at 80 mm Hg and regenerated kidneys perfused at 120 mm Hg (regenerated*). Decellularized kidneys showed a polyuric state while regenerated constructs were relatively oliguric compared to cadaveric kidneys. **(c)** Bar graph showing the average creatinine clearance in cadaveric, decellularized and regenerated kidneys perfused at 80 mm Hg and regenerated kidneys perfused at 120 mm Hg (regenerated*). With increased perfusion pressure creatinine clearance in regenerated kidneys improved. **(d)** Bar graph showing vascular resistance of cadaveric decellularized and regenerated kidneys showing an increase in vascular resistance with decellularization and partial recovery in regenerated kidneys. Error bars, s.d. **(b–d)**. **(e)** Photograph of rat peritoneum after laparotomy, left nephrectomy and orthotopic transplantation of a regenerated left kidney construct. The recipient left renal artery and left renal vein are connected to the regenerated kidney's renal artery and vein. The regenerated kidney's ureter remained cannulated for collection of urine production after implantation (left). Right, photograph of the transplanted regenerated kidney construct after unclamping of left renal artery and renal vein showing homogeneous perfusion of the graft without signs of bleeding. **(f)** Composite histologic image of a transplanted regenerated kidney confirming perfusion across the entire kidney cross section and the absence of parenchymal bleeding. Scale bar, 500 μm .



and transplanted regenerated left kidneys in an orthotopic position. We anastomosed regenerated left kidneys to the recipient's renal artery and vein (Fig. 4e). Throughout the entire test period, regenerated kidney grafts seemed well perfused without any evidence of bleeding from the vasculature, collecting system or parenchyma (Fig. 4e). The ureter remained cannulated to document *in vivo* production of clear urine without evidence of gross hematuria and to collect urine samples. Regenerated kidneys produced urine from shortly after the unclamping of recipient vasculature until the planned termination of the experiment. Histological evaluation of explanted regenerated kidneys showed blood-perfused vasculature without evidence of parenchymal bleeding or microvascular thrombus formation (Fig. 4f).

Corresponding to the *in vitro* studies, decellularized kidneys produced a filtrate that was high in glucose ($249 \pm 62.9 \text{ mg dl}^{-1}$ (mean \pm s.d.) compared to $29 \pm 8.5 \text{ mg dl}^{-1}$ in native controls) and albumin ($26.85 \pm 4.03 \text{ g dl}^{-1}$ compared to $0.6 \pm 0.4 \text{ g dl}^{-1}$ in controls) but low in urea ($18 \pm 42.2 \text{ mg dl}^{-1}$ compared to $617.3 \pm 34.8 \text{ mg dl}^{-1}$ in controls) and creatinine ($0.5 \pm 0.3 \text{ mg dl}^{-1}$ compared to $24.6 \pm 5.8 \text{ mg dl}^{-1}$ in controls). Regenerated kidneys produced less urine than native kidneys ($1.2 \pm 0.1 \mu\text{l min}^{-1}$ (mean \pm s.d.) compared to $3.2 \pm 0.9 \mu\text{l min}^{-1}$ in native controls and $4.9 \pm 1.4 \mu\text{l min}^{-1}$ in decellularized kidneys) with lower creatinine ($1.3 \pm 0.2 \text{ mg dl}^{-1}$) and urea ($28.3 \pm 8.5 \text{ mg dl}^{-1}$) than native controls but showed improved glucosuria ($160 \pm 20 \text{ mg dl}^{-1}$) and albuminuria ($4.67 \pm 2.51 \text{ g l}^{-1}$) when compared to decellularized kidneys. Also consistent with the *in vitro* results, creatinine clearance in regenerated kidneys was lower than that in native kidneys ($0.01 \pm 0.002 \text{ ml min}^{-1}$ compared to $0.36 \pm 0.09 \text{ ml min}^{-1}$ in controls), as was urea excretion ($0.003 \pm 0.001 \text{ mg min}^{-1}$ compared to $0.19 \pm 0.01 \text{ mg min}^{-1}$ in controls). Orthotopic transplantation of regenerated kidneys showed immediate graft function during blood perfusion through the recipient's vasculature *in vivo* without signs of clot formation or bleeding. Results of urinalysis corresponded to the *in vitro* observation of the relative immaturity of the constructs.

DISCUSSION

A bioengineered kidney derived from patient-derived cells and regenerated 'on demand' for transplantation could provide an alternative treatment for patients suffering from renal failure. Although many hurdles remain, we describe a new approach for the creation of such a

graft and report three milestones: the generation of three-dimensional acellular renal scaffolds using perfusion decellularization of cadaveric rat, porcine and human kidneys; the repopulation of endothelial and epithelial compartments of such renal scaffolds, leading to the formation of viable tissue; and excretory function of the resulting graft during perfusion through its vasculature *in vitro* and after orthotopic transplantation *in vivo*.

In line with previous studies, we confirmed that detergent decellularization of whole rat, porcine and human kidneys removes cells and cellular debris without disruption of vascular, glomerular and tubular ultrastructure^{14,16–18}. Decellularization led to a loss of cell-mediated functions such as macromolecular sieving and solute transport. Glomerular and tubular basement membranes are permeable to macromolecules, small solutes and water because filtration and reabsorption occur across these barriers in the native kidney^{21,24}. Because macromolecule retention, secretion and reabsorption of metabolites and electrolytes and regulation of an acid-base equilibrium depend on viable endothelium and epithelium, we repopulated acellular scaffolds with endothelial and immature epithelial cells²⁵. Whereas cell seeding of tissues such as muscle, vasculature or trachea can be accomplished by surface attachment or intraparenchymal injection, repopulation of a more complex organ such as the kidney poses numerous challenges^{26,27}. Similarly to in our previous experiments with lungs, we took advantage of pre-existing vascular and urinary compartments and seeded endothelial cells through the vascular tree and epithelial cells through the collecting system¹³. The length and diameter of the acellular nephrons posed a major challenge to cell seeding from the urinary side. Tubule elasticity and permeability increase with decellularization, whereas tubular diameters increase with pressure²¹. Here a transrenal pressure gradient during the initial cell seeding substantially increased cell delivery and retention. Glomerular ECM structures predominantly repopulated with podocytes, whereas tubular structures repopulated with tubular epithelial cells with reestablished polarity. Such site-selective engraftment of podocytes on glomerular basement membranes highlights the value of native ECM in tissue regeneration. Laminins and collagen IV are the major ECM proteins of the glomerular basement membrane and are necessary for podocyte adhesion, slit diaphragm formation and glomerular barrier function^{28,29}. Immunohistochemical staining of matrix cross

sections in our study showed preservation of these proteins within the glomerular basement membrane after perfusion decellularization. *In vitro*, $\alpha 3 \beta 1$ integrin mediates rat podocyte adhesion and regulates anchorage-dependent growth and cell-cycle control^{30,31}. Preserved glomerular basement membrane proteins in decellularized kidney scaffolds and β -1 integrin expression in engrafted podocytes suggest site-specific cell adhesion to physiologic ECM domains.

After several days in organ culture, regenerated kidney constructs produced urine *in vitro*. The intact whole-organ architecture of regenerated kidneys provided a unique opportunity for global functional testing and assessment of *in vivo* function after transplantation. In regenerated kidneys, macromolecular sieving, glucose and electrolyte reabsorption were partially restored, indicating engraftment and function of endothelial cells, podocytes and tubular epithelial cells. The glomerular filtration rate in regenerated kidneys was lower compared to in cadaveric kidneys, which was in part a result of increased vascular resistance leading to decreased graft perfusion. Creatinine clearance improved with increased renal arterial perfusion pressures. Fractional reabsorption of electrolytes did not reach the levels of cadaveric kidneys, which could be related to incomplete seeding and the immature stage of seeded neonatal epithelial cells²². Further maturation of the cell-seeded constructs will probably improve vascular patency and control of electrolyte reabsorption²⁸. Despite this functional immaturity, regenerated kidney constructs provided urine production and clearance of metabolites after transplantation *in vivo*. We did not observe bleeding or graft thrombosis during perfusion through the recipient's vascular system. Successful orthotopic transplantation in rats demonstrates the advantage of physiologic graft size and anatomic features such as renal vascular conduits and ureter. Once developed further, bioengineered kidneys could become a fully implantable treatment option for renal support in end-stage kidney disease.

In summary, cadaveric kidneys can be decellularized, repopulated with endothelial and epithelial cells, matured to functional kidney constructs *in vitro* and transplanted in an orthotopic position to provide excretory function *in vivo*. Translation of this technology beyond proof of principle will require the optimization of cell-seeding protocols to human-sized scaffolds and an upscaling of biomimetic organ culture, as well as the isolation, differentiation and expansion of the required cell types from clinically feasible sources.

METHODS

Methods and any associated references are available in the [online version of the paper](#).

Note: Supplementary information is available in the [online version of the paper](#).

ACKNOWLEDGMENTS

The present study was supported by the US National Institutes of Health (NIH) Director's New Innovator Award DP2 OD008749-01 and departmental funds. J.J.S. was supported by an AQA Research Fellowship and an American Heart Association Predoctoral Fellowship. The Program in Membrane Biology Microscopy Core is supported by NIH grants DK43351 and DK57521. We further thank Q.C. Ott for critical review and editing of the manuscript. We thank C. Hoffman, J. Beagle and M. Duggan for technical support with urine sample analysis. We thank M. McKee for her expert support with transmission electron microscopy and A. Tisdale for her expert support with scanning electron microscopy.

AUTHOR CONTRIBUTIONS

H.C.O. conceived, designed and oversaw all of the studies, collection of results, interpretation of the data and writing of the manuscript and was also responsible for the primary undertaking, completion and supervision of all experiments. J.J.S. and J.P.G. performed animal surgeries, conducted decellularization and whole-organ culture experiments and performed *in vitro* and *in vivo* testing. S.E.G. was responsible for cell culture, preparation of cell suspensions and matrix

characterization. G.G. characterized fetal lung cells and scaffolds and regenerated constructs using various imaging techniques. J.P.V. provided input on tissue engineering aspects and reviewed the manuscript.

COMPETING FINANCIAL INTERESTS

The authors declare no competing financial interests.

Reprints and permissions information is available online at <http://www.nature.com/reprints/index.html>.

- Centers for Disease Control and Prevention. National chronic kidney disease fact sheet: general information and national estimates on chronic kidney disease in the United States, 2010. (<http://www.cdc.gov/DIABETES/pubs/factsheets/kidney.htm>) (2010).
- US Department of Health and Human Services. National transplantation data report. OPTN: Data Organ Procurement and Transplantation Network. (<http://optn.transplant.hrsa.gov/latestData/step2.asp?>) (2013).
- Kawai, T. *et al.* HLA-mismatched renal transplantation without maintenance immunosuppression. *N. Engl. J. Med.* **358**, 353–361 (2008).
- Humes, H.D., Krauss, J.C., Cieslinski, D.A. & Funke, A.J. Tubulogenesis from isolated single cells of adult mammalian kidney: clonal analysis with a recombinant retrovirus. *Am. J. Physiol.* **271**, F42–F49 (1996).
- Humes, H.D., MacKay, S.M., Funke, A.J. & Buffington, D.A. Tissue engineering of a bioartificial renal tubule assist device: *in vitro* transport and metabolic characteristics. *Kidney Int.* **55**, 2502–2514 (1999).
- Humes, H.D., Buffington, D.A., MacKay, S.M., Funke, A.J. & Weitzel, W.F. Replacement of renal function in uremic animals with a tissue-engineered kidney. *Nat. Biotechnol.* **17**, 451–455 (1999).
- Humes, H.D. *et al.* Initial clinical results of the bioartificial kidney containing human cells in ICU patients with acute renal failure. *Kidney Int.* **66**, 1578–1588 (2004).
- Humes, H.D., Weitzel, W.F. & Fissell, W.H. Renal cell therapy in the treatment of patients with acute and chronic renal failure. *Blood Purif.* **22**, 60–72 (2004).
- Rogers, S.A. & Hammerman, M.R. Prolongation of life in anephric rats following *de novo* renal organogenesis. *Organogenesis* **1**, 22–25 (2004).
- Gura, V., Macy, A.S., Beizai, M., Ezon, C. & Golper, T.A. Technical breakthroughs in the wearable artificial kidney (WAK). *Clin. J. Am. Soc. Nephrol.* **4**, 1441–1448 (2009).
- Fissell, W.H. & Roy, S. The implantable artificial kidney. *Semin. Dial.* **22**, 665–670 (2009).
- Atala, A., Bauer, S.B., Soker, S., Yoo, J.J. & Retik, A.B. Tissue-engineered autologous bladders for patients needing cystoplasty. *Lancet* **367**, 1241–1246 (2006).
- Ott, H.C. *et al.* Perfusion-decellularized matrix: using nature's platform to engineer a bioartificial heart. *Nat. Med.* **14**, 213–221 (2008).
- Ott, H.C. *et al.* Regeneration and orthotopic transplantation of a bioartificial lung. *Nat. Med.* **16**, 927–933 (2010).
- Nakayama, K.H., Batchelder, C.A., Lee, C.I. & Tarantal, A.F. Decellularized rhesus monkey kidney as a three-dimensional scaffold for renal tissue engineering. *Tissue Eng. Part A* **16**, 2207–2216 (2010).
- Ross, E.A. *et al.* Embryonic stem cells proliferate and differentiate when seeded into kidney scaffolds. *J. Am. Soc. Nephrol.* **20**, 2338–2347 (2009).
- Orlando, G. *et al.* Production and implantation of renal extracellular matrix scaffolds from porcine kidneys as a platform for renal bioengineering investigations. *Ann. Surg.* **256**, 363–370 (2012).
- Song, J.J. & Ott, H.C. Organ engineering based on decellularized matrix scaffolds. *Trends Mol. Med.* **17**, 424–432 (2011).
- Sullivan, D.C. *et al.* Decellularization methods of porcine kidneys for whole organ engineering using a high-throughput system. *Biomaterials* **33**, 7756–7764 (2012).
- Olivetti, G., Anversa, P., Rigamonti, W., Vitali-Mazza, L. & Loud, A.V. Morphometry of the renal corpuscle during normal postnatal growth and compensatory hypertrophy. A light microscope study. *J. Cell Biol.* **75**, 573–585 (1977).
- Welling, L.W. & Grantham, J.J. Physical properties of isolated perfused renal tubules and tubular basement membranes. *J. Clin. Invest.* **51**, 1063–1075 (1972).
- Falk, G. Maturation of renal function in infant rats. *Am. J. Physiol.* **181**, 157–170 (1955).
- Bray, J. & Robinson, G.B. Influence of charge on filtration across renal basement membrane films *in vitro*. *Kidney Int.* **25**, 527–533 (1984).
- Deen, W.M., Lazzara, M.J. & Myers, B.D. Structural determinants of glomerular permeability. *Am. J. Physiol. Renal Physiol.* **281**, F579–F596 (2001).
- Humes, H.D. Acute renal failure: prevailing challenges and prospects for the future. *Kidney Int. Suppl.* **50**, S26–S32 (1995).
- Quint, C. *et al.* Decellularized tissue-engineered blood vessel as an arterial conduit. *Proc. Natl. Acad. Sci. USA* **108**, 9214–9219 (2011).
- Elliott, M.J. *et al.* Stem-cell-based, tissue engineered tracheal replacement in a child: a 2-year follow-up study. *Lancet* **380**, 994–1000 (2012).
- Dandapani, S.V. *et al.* α -actinin-4 is required for normal podocyte adhesion. *J. Biol. Chem.* **282**, 467–477 (2007).
- Kretzler, M. Regulation of adhesive interaction between podocytes and glomerular basement membrane. *Microsc. Res. Tech.* **57**, 247–253 (2002).
- Cybulsky, A.V., Carbonetto, S., Huang, Q., McTavish, A.J. & Cyr, M.D. Adhesion of rat glomerular epithelial cells to extracellular matrices: role of $\beta 1$ integrins. *Kidney Int.* **42**, 1099–1106 (1992).
- Borza, C.M. *et al.* Human podocytes adhere to the KRGDS motif of the $\alpha 3 \alpha 4 \alpha 5$ collagen IV network. *J. Am. Soc. Nephrol.* **19**, 677–684 (2008).

ONLINE METHODS

Perfusion decellularization of kidneys. We isolated 68 rat kidneys for perfusion decellularization. All animal experiments were performed in accordance with the Animal Welfare Act and approved by the institutional animal care and use committee at Massachusetts General Hospital. We anesthetized male, 12-week-old Sprague-Dawley rats (Charles River Labs) using inhaled 5% isoflurane (Baxter). After systemic heparinization (American Pharmaceutical Partners) through the infrahepatic inferior vena cava, a median laparotomy exposed the retroperitoneum. After removal of the Gerota's fascia, perirenal fat and kidney capsule, we transected the renal artery, vein and ureter and retrieved the kidney from the abdomen. We cannulated the ureter with a 25-gauge cannula (Harvard Apparatus). Then we cannulated the renal artery with a prefilled 25-gauge cannula (Harvard Apparatus) to allow antegrade arterial perfusion of heparinized PBS (Invitrogen) at 30 mm Hg arterial pressure for 15 min to rid the kidney of residual blood. We then administered decellularization solutions at 30 mm Hg of constant pressure in the following order: 12 h of 1% SDS (Fisher) in deionized water, 15 min of deionized water and 30 min of 1% Triton X-100 (Sigma) in deionized water. After decellularization, we washed the kidney scaffolds with PBS containing 10,000 U/ml penicillin G, 10 mg/ml streptomycin and 25 µg/ml amphotericin B (Sigma) at 1.5 ml per min constant arterial perfusion for 96 h.

Rat neonatal kidney cell isolation. We euthanized day 2.5–3.0 Sprague-Dawley neonates for organ harvests. We then excised both kidneys by median laparotomy and stored them on ice (4 °C) in renal epithelial growth medium (REGM, Lonza). We transferred kidneys to a 100-mm culture dish (Corning) for residual connective tissue removal and subsequent mincing into <1 mm³ pieces. The renal tissue slurry was resuspended in 1 mg/ml collagenase I (Invitrogen) and 1 mg/ml dispase (StemCell Technologies) in DMEM (Invitrogen) and incubated in a 37 °C shaker for 30 min. The resulting digest slurry was strained (100 µm; Fisher) and washed with 4 °C REGM. We then resuspended nonstrained tissue digested in collagenase and dispase as described above and repeated the incubation, straining and blocking. The resulting cell solution was centrifuged (200g, 5 min), and cell pellets were resuspended in 2.5 ml REGM, counted and seeded into acellular kidney scaffolds as described below.

HUVEC subculture and preparation. We expanded mCherry-labeled HUVECs at passages 8–10 on gelatin A-coated (BD Biosciences) cell-culture plastic and grew the cells with endothelial growth medium-2 (EGM2, Lonza). At the time of seeding, cells were trypsinized, centrifuged, resuspended in 2.0 ml of EGM2, counted and subsequently seeded into decellularized kidneys as described below.

Cell seeding. We trypsinized and diluted $50.67 \times 10^6 \pm 12.84 \times 10^6$ (mean \pm s.d.) HUVECs in 2.0 ml EGM2 and seeded these onto the acellular kidney scaffold through the arterial cannula at a constant flow of 1.0 ml per min. Cells were allowed to attach overnight, after which perfusion culture resumed. Following the procedure above, $60.71 \times 10^6 \pm 11.67 \times 10^6$ rat neonatal kidney cells were isolated, counted and resuspended in 2.5 ml of REGM. The cell suspension was seeded through the ureter cannula after subjecting the organ chamber to a –40 cm H₂O pressure. Cells were allowed to attach overnight, after which perfusion culture resumed.

Bioreactor design and whole-organ culture. We designed and custom built the kidney bioreactor as a closed system that could be gas sterilized after cleaning and assembly, needing only to be opened once at the time of organ placement. Perfusion media and cell suspensions were infused through sterile access ports (Cole-Parmer) to minimize the risk of contamination. Media was allowed to equilibrate with 5% CO₂ and 95% room air by flowing through a silicone tube oxygenator (Cole-Parmer) before reaching the cannulated renal artery at 1.5 ml per min. The ureter and vein were allowed to drain passively into the reservoir during the biomimetic culture.

Isolated kidney experiments. To assess *in vitro* kidney function, we perfused single native, regenerated and decellularized kidneys with 0.22 µm-filtered

(Fisher) Krebs-Henseleit solution containing NaHCO₃ (25.0 mM), NaCl (118 mM), KCl (4.7 mM), MgSO₄ (1.2 mM), NaH₂PO₄ (1.2 mM), CaCl₂ (1.2 mM), BSA (5.0 g/dl), D-glucose (100 mg/dl), urea (12 mg/dl) and creatinine (20 mg/dl), (Sigma-Aldrich). We added the amino acids glycine (750 mg/l), L-alanine (890 mg/l), L-asparagine (1,320 mg/l), L-aspartic acid (1,330 mg/l), L-glutamic acid (1,470 mg/l), L-proline (1,150 mg/l) and L-serine (1,050 mg/l) before testing (Invitrogen). Krebs-Henseleit solution was oxygenated (5% CO₂ and 95% O₂), warmed (37 °C) and perfused through the arterial cannula at constant pressures of 80–120 mm Hg without recirculation. Urine and venous effluent passively drained into separate collection tubes. We took samples at 10, 20, 30, 40 and 50 min after initiating perfusion and froze them immediately at –80 °C until analysis. Urine, venous effluent and perfusing Krebs-Henseleit solutions were quantified using a Catalyst Dx Chemistry Analyzer (IDEXX). We calculated the vascular resistance (RVR) as arterial pressure (mm Hg)/renal blood flow (ml/g/min). After completion of *in vitro* experiments, we flushed kidneys with sterile PBS, decannulated them and transferred to a sterile container in cold (4 °C) PBS until further processing.

Histology, immunofluorescence and immunohistochemistry. We processed native, decellularized and regenerated kidneys following the identical fixation protocol for paraffin embedding (5% formalin buffered PBS; Fisher) for 24 h at room temperature, and the sections to be frozen were fixed overnight in 4% paraformaldehyde (Fisher) at 4 °C. We embedded sections in paraffin or Tissue Tek Optimal Cutting Temperature (OCT) compound (VWR) for sectioning following standard protocols. Tissue sections were cut into 5-µm sections, and H&E staining was performed (Sigma-Aldrich) using standard protocols. Sections were also stained with Movat's pentachrome (American Mastertech) following the manufacturer's protocol.

Paraffin-embedded sections underwent deparaffinization with two changes of xylene (5 min), two changes of 100% ethanol (3 min) and two changes of 95% ethanol (3 min) and were placed in deionized water (solutions all from Fisher). For immunostaining, deparaffinized slides first underwent antigen retrieval in heated (95 °C) sodium citrate buffer solution, pH 6.0 (Dako), for 20 min and were then allowed to cool to room temperature for 20 min. For immunostaining of collagen IV, elastin and laminin epitopes, slides were blocked for 5 min in PBS and then incubated with 20 mg/ml Proteinase K (Sigma) in TE (Tris and EDTA) buffer, pH 8.0, at 37 °C for 10 min. After a 5-min block in PBS, slides received Dual Endogenous Enzyme-Blocking Reagent (Dako) for 5 min and then blocking buffer (1% BSA and 0.1% Triton X-100 in PBS; Sigma) for 30 min. Primary antibodies were allowed to attach overnight at 4 °C. Primary antibody dilutions were made with blocking buffer and were as follows: 1:50 antibody to elastin (Santa Cruz Biotechnology, sc-17581), 1:50 antibody to laminin Y-1 (B-4) (Santa Cruz Biotechnology, sc-13144), 1:50 antibody to collagen IV (Lifespan Bioscience, LS-C79592), 1:200 antibody to podocin (Abcam, ab50339), 1:200 antibody to Na/K-ATPase (Abcam, ab7671) and 1:200 antibody to E-cadherin (BD Biosciences, 610181). After primary antibody incubation, slides were washed in PBS for 5 min, and a secondary antibody conjugated to horseradish peroxidase (HRP) was added at 1:100 for 30 min (Dako). The resulting slides were washed with PBS and developed with 3,3'-diaminobenzidine (Dako) until good staining intensity was observed. Nuclei were counterstained with hematoxylin (Sigma). A coverslip was mounted using permount (Fisher) after dehydration with a sequential alcohol gradient and xylene (Fisher).

For immunofluorescence, paraffin-embedded sections underwent deparaffinization and antigen retrieval and received primary antibody dilutions prepared in blocking buffer as described above. After primary antibody addition, slides were blocked as described above. Fluorescent secondary antibodies, all 1:250 diluted in blocking buffer (anti-species conjugated to Alexa fluorophores; Invitrogen) were allowed to attach for 45 min. Nuclei were counterstained with DAPI (Invitrogen) and coverslip (Fisher) mounted using ProLong Gold antifade reagent (Invitrogen, P36930).

Omission of primary antibody and species immunoglobulin G1 antibody (Vector Labs) served as negative controls for both immunohistochemistry and immunofluorescence. Immunohistochemistry, H&E- and pentachrome-stained images were recorded using a Nikon Eclipse TE200 microscope (Nikon), and immunofluorescent images were recorded using a Nikon A1R-A1 confocal microscope (Nikon).

Transmission electron microscopy. Tissues were fixed in 2.0% glutaraldehyde in 0.1 M sodium cacodylate buffer, pH 7.4, overnight at 4 °C, rinsed, post fixed in 1.0% osmium tetroxide in cacodylate buffer for 1 h at room temperature and rinsed (Electron Microscopy Sciences). Then sections were dehydrated through a graded series of ethanol and infiltrated with Epon resin (Ted Pella) in a 1:1 solution of Epon and ethanol overnight. Sections were then placed in fresh Epon for several hours and embedded in Epon overnight at 60 °C. Thin sections were cut on a UC6 ultramicrotome (Leica), collected on formvar-coated grids, stained with uranyl acetate and lead citrate and examined in a JEM 1011 transmission electron microscope at 80 kV (Jeol). Images were collected using an AMT digital imaging system (Advanced Microscopy Techniques).

SDS, DNA collagen and sulfated glycosaminoglycans (sGAG) quantification. SDS was quantified using Stains-All Dye (Sigma) as previously described³⁰. Briefly, lyophilized tissues were digested in collagenase buffer (Sigma) for 48 h at 37 °C with gentle rotation. Digest supernatants (1 μ l) containing any residual SDS were then added to 4 ml of a working Stains-All Dye solution, and absorbance was measured at 488 nm. DNA was quantified using the Quanti-iT PicoGreen dsDNA kit (Invitrogen). Briefly, DNA was extracted from lyophilized tissue samples in Tris-HCl buffer with Proteinase K (200 μ g/ml; Sigma) for 3 h at 37 °C with gentle rotation. Digest supernatants (10 μ l) were diluted in TE buffer and then mixed with prepared PicoGreen reagent. Samples were excited at 480 nm, and fluorescence was measured at 520 nm. Soluble collagen was quantified using the Sircol Assay (Biocolor), as per the manufacturer's instructions. Lyophilized tissue samples were first subjected to acid-pepsin collagen extraction overnight at 4 °C and then to overnight isolation and concentration. Assay was then performed as instructed. sGAG were quantified using the Blyscan Assay (Biocolor). Before measurement, sGAG were extracted using a papain extraction reagent (Sigma) and heated for 3 h at 65 °C. Assay was then performed as instructed. All concentrations were determined on the basis of a standard curve generated in parallel, and values were normalized to original tissue dry weight.

Chemical analysis of blood and urine samples. Blood and urine chemistries were analyzed using a Catalyst Dx Chemistry Analyzer (IDEXX Laboratories) integrated with an IDEXX VetLab Station for comprehensive sample and data management. As per the manufacturer's protocol, 700 μ l was analyzed for each blood sample, and 300 μ l was analyzed for each urine sample. When necessary, urine samples were diluted on the basis of the urine volume collected and then diluent was added for a sample volume of 300 μ l, and the results account for any dilution calculations. Blood samples were first passed through a lithium heparin whole-blood separator before being analyzed, and no dilutions were needed for these samples. All samples were passed through proprietary IDEXX diagnostic CLIPs Chem 10 (ALB, ALB/GLOB, ALKP, ALT, BUN, BUN/CREA, CREA, GLOB, GLU and TP) and Lyte 4 (Cl, K, Na and Na/K), as well as single diagnostic slides for magnesium, calcium and phosphate.

Morphometric quantification of glomeruli. Ten low-powered fields (4 \times) were randomly selected from the subcapsular and juxtamedullary regions of

H&E-stained sections (5 μ m) of native, decellularized and regenerated kidneys ($n = 3$ in each group). Glomeruli were counted in each of the ten fields to determine the average number of glomeruli per section, and the numbers of glomeruli per section in experiments from the same group were used to determine the mean glomeruli in each type of kidney (mean \pm s.e.m.). Reseeded glomeruli in regenerated kidneys were counted as a subset in each of the ten low-powered fields and then averaged per experiment. The percentage of reseeded glomeruli for each experiment was calculated using the average number of reseeded glomeruli compared to the average number of glomeruli per section and used to calculate the mean percentage of reseeded glomeruli in regenerated kidneys (mean percentage \pm s.e.m.). Ten high-powered fields (20 \times) of individual glomeruli from the same H&E-stained sections of native, decellularized and regenerated kidneys were used for morphometric analysis ($n = 3$ in each group). All morphometric measurements were determined using ImageJ (NIH). For each of the individual glomeruli, both the long- and short-axes diameters of the renal corpuscle were measured. Bowman's space was determined by subtracting the area measured around the inner surface of the Bowman's capsule from the area measured around the outer surface of the glomerular capillary bed. All measurements were averaged per experiment, and experiments from the same group were used to determine mean values \pm s.e.m.

Organ preparation and orthotopic transplantation. Native, decellularized or regenerated kidneys were treated identically with the exception that native kidneys were harvested from anesthetized (5% inhaled isoflurane), 12-week-old male Sprague-Dawley rats after systemic heparinization. Native kidneys were exposed and harvested identically as described above for perfusion decellularization with the exception that the left renal artery was flushed with 4 °C Belzer UW Cold Storage Solution (Bridge to Life) at 1 ml/min for 5 min before surgical manipulation of the kidney and rinsed with 20 ml sterile 4 °C PBS before implantation.

Kidney grafts were prepared for orthotopic transplantation by dissecting the hilar structures (artery, vein and ureter) circumferentially on ice. The graft renal artery and vein were cuffed using a modified cuff technique described previously¹⁷ with 24-G and 20-G, respectively, FEP polymer custom-made cuffs (Smith-Medical). For *in vivo* experiments, 10-week-old (220–225 g) NIH-RNU-M recipient rats (Taconic Farms) underwent 5% inhaled isoflurane induction and were maintained with ventilated 1–3% inhaled isoflurane through a 16-G endotracheal tube (BD Biosciences). Rats were placed supine on a heating pad (Sunbeam). After a median laparotomy and systemic heparinization through the right renal vein, the left recipient renal artery, vein and ureter were identified, dissected circumferentially and incised close to the left hilum, sparing the left suprarenal artery. The left renal artery and vein were then clamped using a micro-serrefine clamp (Fine Science Tools). The left kidney was then carefully separated from the Gerota's fascia and removed. The regenerated kidney graft artery and venous cuffs were inserted into the recipient's vessels and secured with a 6-0 silk ligation (Fine Science Tools). The recipient artery and vein were then unclamped, and patent anastomoses were confirmed. Urine was allowed to drain passively from the ureter through a 25-G angiocath (Harvard Apparatus). Cadaveric orthotopic kidney transplants and decellularized kidney transplants served as controls.